# Shedding light onto the nano- and micro-structures of B-containing SiOC glasses using high resolution TEM 3D imaging

Simona Moldovan, Ovidiu Ersen, Clément Sanchez, Renzo Campostrini, Gian Domenico Sorarù

Version of Record: https://www.sciencedirect.com/science/article/pii/S0955221919302031
Manuscript_44c160d0b5bf08fce662902c982e30fe

# *Shedding light onto the nano- and micro-structures of B-containing SiOC glasses using high resolution TEM 3D imaging*

Simona Moldovan[1,2], Ovidiu Ersen[1,3,*], Clément Sanchez[4],

Renzo Campostrini[5], Gian Domenico Sorarù[5,*]

[1]*Institut de Physique et Chimie des Matériaux de Strasbourg, UMR 7504 CNRS – Université de Strasbourg, 23 rue du LOESS, BP 43, Strasbourg Cedex 2, France*

[2]*Groupe de Physique des Matériaux, UMR CNRS 6634, Université de Rouen, INSA Rouen, Avenue de l'Université, Saint Etienne du Rouvray, France*

[3]*Institut Universitaire de France (IUF), Paris, France*

[4]*Sorbonne Université, Collège de France, PSL University, CNRS, Laboratoire de Chimie de la Matière Condensée de Paris (LCMCP), F-75005 Paris*

[5]*University of Trento, Department of Industrial Engineering, Via Sommarive 9, 38123 Trento, Italy*

[*]*Corresponding authors: ovidiu.ersen@ipcms.unistra.fr, giandomenico.soraru@unitn.it*

## Abstract

The internal structure of nanostructured pyrolyzed SiBOC glasses has been analyzed using a combination of transmission electron microscopy techniques including high resolution imaging, EELS spectroscopy and 3D imaging. For the first time, we provide direct information on the 3D architecture within such complex glasses containing SiC nanograins, silica-rich and carbon nanodomains. Their sizes and relative 3D distribution have been precisely quantified. It was shown that the SiC nanocrystals and the silica-rich domains exhibit different types of connectivities with the graphitic carbon network. A direct evidence of the existence of "covalent" bridges between the edges of graphitic nanoplatelets and the SiC nanocrystals is provided. In addition, it was demonstrated that the silica rich domains are not covalently bonded to the graphitic platelets. As a consequence, this amorphous phase can be dissolved into HF and may generate a bimodal porosity, in strong relationship with the initial nanostructure of the SiBOC glass specimen.

## 1. Introduction

Silicon oxycarbides (SiOCs) are amorphous silica-based ceramics derived from polysiloxane resins through a pyrolysis process in inert atmosphere [1,2]. Compared to the parent silica glass, the insertion of C into the network results in superior mechanical and thermal properties [3] and increases the glass transition temperature up to 1350°C [4]. In the last 20 years the structure of these glasses has been the subject of many studies and, as a result, the whole scientific community agrees on the following structural features: (i) Si-O, Si-C($sp^3$) and $sp^2$ C=C / $sp^3$ C-C chemical bonds exist in the SiOC structure [5]; (ii) the local environment around the Si atoms is well represented by mixed silicon-centered tetrahedra in which Si atoms are bonded at the same time with O and C atoms [6]. The mixed silicon sites are particularly abundant at low pyrolysis temperature (1000°C) and then, by further increasing the maximum temperature from 1000 up to 1400°C a redistribution reaction between Si-O/Si-C bonds occurs leading to the formation of $SiC_4$ units (belonging to nanocrystalline SiC, 2-4 nm sized), and $SiO_4$ units (belonging to an amorphous $SiO_2$-rich phase) [7, 8]. In the same temperature range (1000-1400°C) Raman studies reveal that the free carbon phase undergoes an ordering process with a transformation of $sp^3$ into $sp^2$ C and the formation of turbostratic/nanocrystalline graphite [9]. Finally, residual hydrogen can be present, especially at low pyrolysis temperature, either bonded to C (C-H) and/or Si (Si-H) atoms [10, 11].

In spite of this rather accurate description of the SiOC structure in terms of chemical bonds and local order around the Si atoms, yet the mid-range structure is far from being clearly described and is still a matter of debate among the scientific community. Raj and co-workers proposed a model consisting of clusters of silica tetrahedra encased within an interdomain wall constituted from mixed SiOC bonds, and from a network of $sp^2$ carbon [12]. The model can predict the domain size, estimated from Small Angle X-ray Scatter (SAXS) data, as a function of the carbon and oxygen content. According to this model the mixed Si-O-C units form bonds orthogonally to the $sp^2$ C planes [13]. Another model, similar to the one developed in [12], was proposed by Gregori et al. [14] in which the $sp^2$ C sheets, forming the extended C network and encasing the $SiO_2$ nanodomains, are bonded at their edges via SiC nanoclusters. More recently, Widgeon, Sen and coworkers [15], based on MAS NMR studies, suggested a model, which describes the SiOC nanostructure as a continuous mass fractal backbone of corner-shared $SiC_xO_{4-x}$ tetrahedral units with "voids" occupied by $sp^2$-hybridized graphitic carbon. The oxygen-rich $SiC_xO_{4-x}$ units are located at the interior of this backbone while the carbon-rich units occupy the interface between the backbone and the free carbon nanodomains. Finally Kroll, based on ab-initio molecular dynamic simulations, proposed a model in which the $sp^2$ C layers are bonded at their edges with the surrounding SiOC matrix [16-17].

Unveiling the features of the SiOC mid-range nanostructure - with particular emphasis on the type and chemistry of the interfaces present in these materials - must be regarded not only as a basic science problem but can have important implication in understanding some of the most unique properties of these glasses. For example, the higher thermodynamic stability of silicon oxycarbide glasses compared to the crystalline counterparts (cristobalite, silicon carbide and graphite) has been explained assuming a low free energy of the graphene–silica interfaces containing mixed silicon oxycarbide units [18]. However, a more recent work performed on "pure" hydrogenated silicon oxycarbide glass (with 4.4 mol% H) without free carbon seems to reach a different conclusion since the SiOC sample with 11 mol% $sp^2$ C is less thermodynamically stable than same materials without the extra carbon phase [19]. The nature of the interface between the $sp^2$ C and the SiOC matrix could also

have a role in explaining the high Li-ion capacity of SiOCs when they are used as anode for Li-ion batteries or their semiconducting and piezoresistive behaviors [20, 21, 22] or to explain their HT ultra-low creep behavior [23].

Wilson et al. [24] showed for the first time that HF-etching silicon oxycarbide glasses creates a microscopic pore network due to the dissolution of the $SiO_2$-rich clusters. Since then porous SiOCs obtained through HF attack have been the subject of many studies [25, 26, 27, 28] and the resulting porous C-rich SiOCs have been proposed for different functional applications such as gas sensing and anode for Li-ion batteries [29, 30]. The characterization of the porosity created in SiOC materials via HF etching allows collecting information on the size, amount and distribution of the $SiO_2$-based clusters in the parent SiOC glass, which, otherwise, would be difficult to characterize due to their amorphous nature. Accordingly, it has been shown that the size of $SiO_2$ falls in the range from 1 – 6 nm and is related to the processing temperature and time [25, 31, 32, 33].

In this study, with the aim of precisely solve the microstructure of the SiOC nanostructures, we perform, for the first time, a detailed 3D TEM study of a silicon-(boron)-oxycarbide glass before and after the $SiO_2$ phase has been removed by HF etching. The rationale for studying a B-containing SiOC glass instead of a ternary SiOC is related to the following points:

(i) the structure and the structural evolution of SiBOC glasses is similar to the ternary SiOC system. Boron enters the amorphous silicon oxycarbide network and after pyrolysis at 1200°C in inert atmosphere forms mixed boron oxycarbide units, $BC_yO_{3-y}$, $0 \leq y \leq 3$, which co-exist with the mixed silicon oxycarbide units, $SiC_xO_{4-x}$, $0 \leq x \leq 4$ [34]. At higher temperature the amorphous SiBOC glasses evolves like the ternary SiOC system with a phase separation into an oxide-rich borosilicate phase and nanocrystalline SiC [31];

(ii) there is a known effect of boron in promoting the redistribution reactions between the Si-O/B-O bonds and the Si-C bonds thus leading to a better phase separated glass which will facilitate the structural characterization [32];

(iii) the structure, energetics and electrical properties of SiBOC glasses before and after the HF attack have been deeply studied in our group with complementary techniques and this knowledge will help in discussing the present experimental results [31, 34, 35, 36, 37].

## 2. Experimental methods

B-containing polysiloxane precursor was obtained via a non-hydrolythic sol-gel process starting from methyltriethoxysilane, MTES (ABCR, Karlsruhe, Germany, CAS: 2031-67-6) and boric acid (Carlo Erba, Milan, Italy, CAS: 10043-35-3). The proper amount of $B(OH)_3$ was added to the liquid MTES with a B/Si atomic ratio of 0.5. The system was stirred at 70 °C under reflux until the boric acid was completely dissolved and the solution was poured in plastic test tubes for gelation. After gelation the samples were dried and then pyrolyzed in flowing Ar (100 mL/min) using an alumina tubular furnace at 10 °C/min up to 1400 °C for 1 h. The resulting SiBOC glass was milled in an agate mortar to get fine powders, which were then subjected to the acid attack. Accordingly, 400 mg of SiBOC fine powders were introduced into a polypropylene container and then 50 mL of a HF solution (48 % in water) was added. The container was closed, left at room temperature for 8 h under a gentle stirring. Then, the solution was filtered, the powders were rinsed with distilled

water, dried at 100◦C for 24 h and, at the end, ca 100 mg of etched powders were recovered.

The chemical bonds present in the glass structure before and after HF etching were investigated collecting FT-IR spectra with a Varian 4100 FT-IR Excalibur Series equipment (Lake Forest, CA, USA) in the range 4000 – 400 $cm^{-1}$. The spectra were recorded in transmission mode using KBr pellets with an average of 32 scans and a resolution of 2 $cm^{-1}$.

The B content of the starting SiBOC glass and after HF etching was measured dissolving the samples in a mixture of $HNO_3$, $H_2SO_4$ and HF at 180°C for 12 h using a Parr digestion bomb (Digestion Vessel, mod. 4749, Parr, Moline, IL, USA) according to a published procedure [38]. Then, B concentration was measured by an ICP-OES equipment (SPECTRO Analytical Instruments, Kleve, Germany).

The porosity created by the acid attack was characterized by $N_2$ physisorption technique using an ASAP 2010 (Micromeritics, Norcross, GA, USA) instrument. Before the analysis, the porous SiBOC sample was degased at 200 °C below 1.3 Pa. The specific surface area (SSA) was determined from a BET (Brunauer, Emmet and Teller) analysis in the $P/P_0$ range of 0.05–0.30 using a molecular cross-sectional area for $N_2$ of 0.163 $nm^2$ and a minimum of 5 data points. The pore size distribution was obtained from the adsorption branch of the isotherm through the BJH (Barret, Joyner and Halenda) analysis.

For the TEM experiments, the specimens were dispersed in ethanol and stirred in an ultrasound bath. Prior to the sample deposition, one drop of 5 nm diameter Au nanoparticles (fiducial markers for tomography) were deposited on the suspended carbon membranes. The high-resolution TEM micrographs and the electron tomography experiments were carried out on a Cs-probe corrected Jeol 2100F Transmission Electron Microscope operated at 200kV. The images were recorded on an Ultrascan CCD camera upon 1s exposure for each image. Electron tomography (ET) analyses were performed on the SiBOC glasses prior and after the HF treatment. The ET micrograph series were recorded by specimen tilting along a single axis and the angular range between -70° to 70° was covered using the Saxton tilting scheme, with a step of 1.5°. The images in the series were first aligned using the cross-correlation implemented in IMOD, followed by a manual refinement using the Au NPs as fiducial markers. The volumes were reconstructed using the Algebraic Iterative Reconstruction (ART) methods implemented in TomoJ of the ImageJ software. The volume visualization and analyses were carried out in Fiji/ImageJ.

The Energy Filtered TEM (EFTEM) and Electron Energy Loss Spectroscopy (EELS) were performed on a double corrected cold-FEG Jeol ARM200 Analytical TEM (GENESIS facility), operated at 200kV and equipped with a Quantum Gatan Imaging Filter. For acquiring the chemical maps in EFTEM, the three-windows method has been employed (one energy window within the corresponding spectra for the signal of interest and two windows for the background extraction) and the exposure times were adapted to each element of interest. The EEL spectra were acquired under Scanning TEM mode using a condenser diaphragm of 40 µm, a 0.1 nm beam with a probe current of 120 pA. For the high resolution (HR) imaging in STEM mode, a High Angular Annular Dark Filed (HAADF) detector has been employed. The camera length employed for the HR imaging was fixed at 8 cm, whilst for the STEM-EELS analyses was fixed at 2 cm and in addition a 2.5 mm aperture was used. Under this configuration, the spatial and spectral resolutions achieved were of 0.1 nm and 0.5 eV, respectively. The EELS spectra were collected in dual EELS mode which allows to acquire simultaneously data of two energy domains. In our case, the signals of Si-$L_{23}$ and C-K edges were used as references, as the corresponding energy domains allowed one to cover the B and O k-lines domains. The EELS spectra were acquired using both a

spectrum-imaging approach (a spectrum is acquired in each pixel of the selected region, in our case a line) and under cumulative mode (the spectra captured adds the signals of spectra collected in each individual pixel).

## 3. Experimental results

### Traditional analyses

Typical FT-IR spectra collected on the SiBOC glass before and after the HF etching process are shown in **Figure 1.** The as pyrolyzed glass, Figure 1a, shows bands at 1090, 660, 465 and a shoulder at 800 $cm^{-1}$ related to the Si-O bonds of the silica matrix, B-O bonds gives rise to the absorption at 1380 $cm^{-1}$ while Si-C bonds of the silicon carbide clusters leads to the peak at 860 $cm^{-1}$. After etching, Figure 1(b), the spectrum is significantly modified: the most intense peak is the one corresponding to the Si-C vibration at 860 $cm^{-1}$. The presence of the $sp^2$ graphitic phase leads to the peak at 1590 $cm^{-1}$ (C=C bonds). The vibration at 1710 $cm^{-1}$ is assigned to C=O moieties, most probably present at the edges of the graphene planes [39]. Less intense peaks at 1400, 1230, 1170 and 460 $cm^{-1}$ are assigned to B-O and Si-O bonds, respectively, and indicate that the HF treatment dissolved almost completely the borosilicate amorphous phase. This result is also supported by the B chemical analysis which indicates that B content decreases from a 3.5 wt%, in the parent SiBOC sample, down to 0.9 wt% after HF attack. In both samples the presence of OH groups leads to a broad band centered at 3500 $cm^{-1}$ (**Fig. SI 1**). Consequently, the comparison of the FT-IR spectra recorded before and after the HF attack, show that the residual porous sample is composed mainly of Si-C and $sp^2$ C=C bonds with only traces of residual Si-O and B-O bonds.

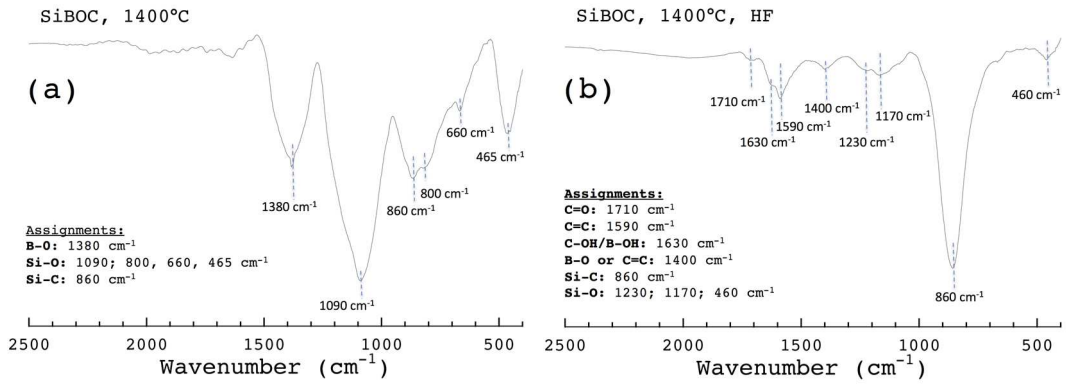


**Figure 1.** FT-IR spectra recorded on the: (a) "as pyrolyzed" SiBOC glass and (b) after HF etching.

The results of the $N_2$ physisorption analysis are shown in **Figure 2**. The adsorption-desorption isotherms (Figure 2a) are of type IV with a hysteresis loop in the range $0.6 \leq P/P_0 \leq 0.8$ caused by the capillary condensation in the mesopore regime (2 - 50 nm). The BET specific surface area is 389 $m^2/g$ with a total pore volume of 0.53 $cm^3/g$. The pore size distribution curve (Figure 2b) shows the formation of pores in the range 2 - 10 nm with a maximum around 6 nm. The results of the $N_2$ physisorption characterization are in agreement with our published studies [32] and confirm that the structure of the silicon oxycarbide glasses contains two interpenetrating nano-sized networks: one $SiO_2$-rich, that can be removed to a great extent by HF etching, and the other one C-rich, that contains the SiC clusters and the free C layers, and that is left behind from the chemical attack.

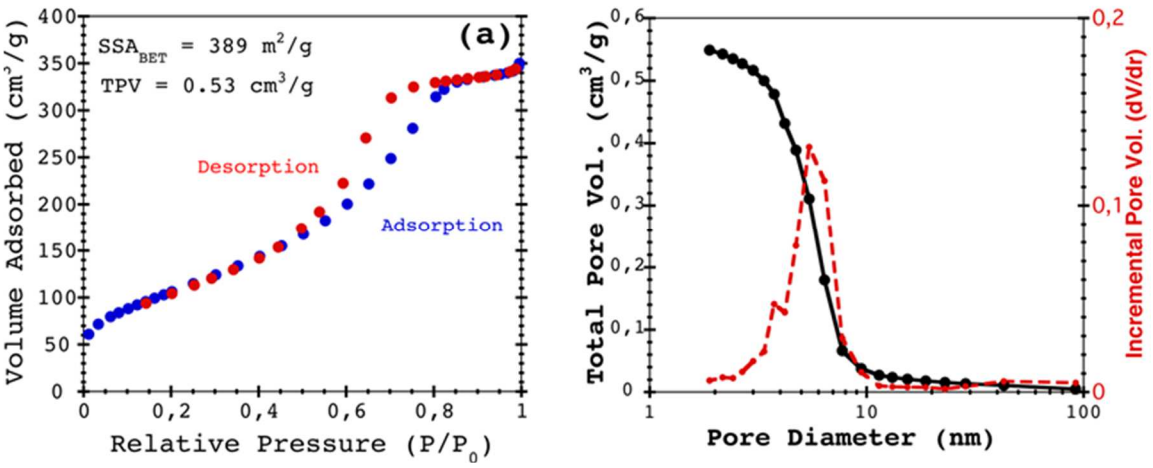


**Figure 2**. $N_2$ physisorption results obtained on the HF-etched SiBOC glasses: (a) $N_2$ adsorption-desorption isotherms and (b) total pore volume and pore size distribution curve.

The microstructure, the mid-range order and the distribution of the chemical elements have been investigated by a combination of TEM-based techniques, including high resolution and Energy Filtered TEM imaging, EELS spectroscopy and electron tomography, all together providing unprecedented and valuable information for the complete evaluation of the materials structure, before and after the HF treatment.

### 2D microstructure of the SiBOC glass before HF etching

The classical TEM analysis and the high resolution images allow us to identify the presence of some SiC nanocrystals (red arrows) and carbon graphitic platelets at the edge of the chosen grains (yellow arrows) within the SiBOC glass (**Figure 3**). Since the thin regions are well-adapted to the high resolution observations, we were able to ascertain the occurrence of lots of crystallographic defects, as indicated by the black arrows in the Figure 3c.

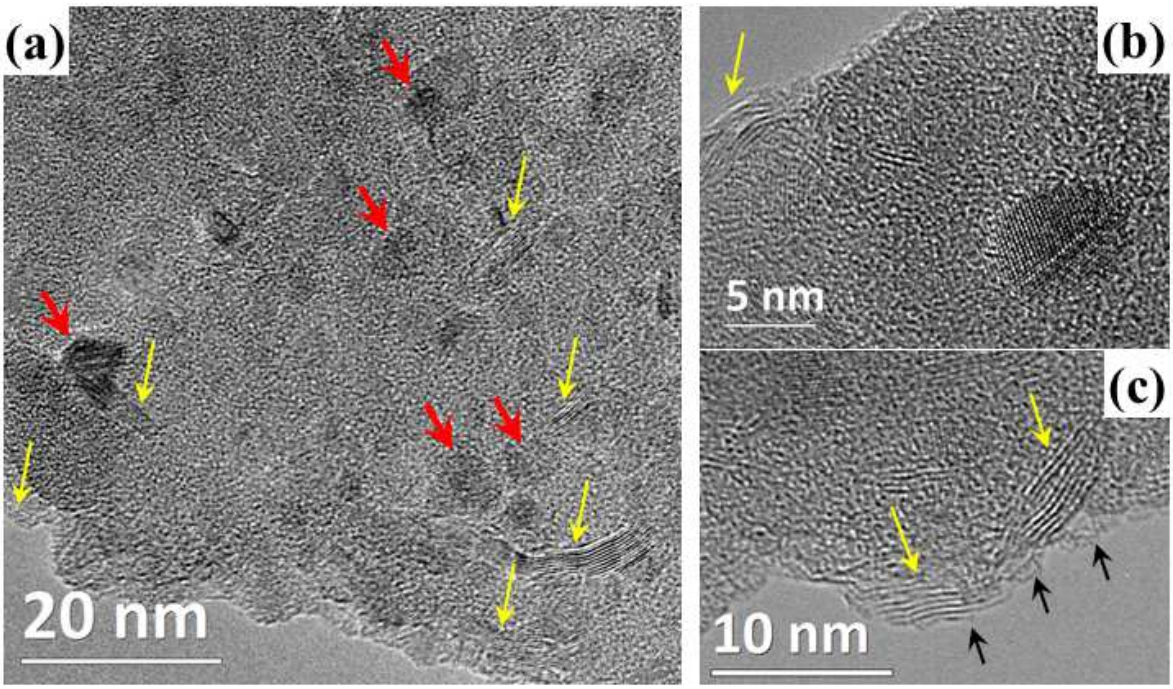


**Figure 3.** TEM micrographs of the SiBOC glasses prior to HF etching treatment. (a) General aspect of the microstructure identifying the presence of crystalline SiC NPs (red arrows) and graphitic

platelets (yellow arrows), the last located at the surface as well as in the bulk of the sample; (b) and (c) higher magnification showing defects present in the graphitic platelets (black arrows).

The spatial distribution of the chemical elements present in the sample prior to the HF treatment was investigated by Energy Filtered TEM (EFTEM). The elemental maps of Si, O, C and B are shown in **Figure 4**. One can observe that the Si and O are homogenously distributed within the structure (the spatial resolution of EFTEM is estimated here at about few nanometers). However, the C distribution appears to be more heterogeneous as anticipated by the TEM images. Indeed, the occurrence of elongated C platelets revealed by TEM is visible as well in the corresponding elemental maps. However, the lower spatial resolution of the filtered images as compared to the TEM (few nanometers as against few hundreds of pico-meters) did not allow to identify the platelet structure of the C rich areas. The spatial distribution of the boron is much more difficult to estimate particularly in this case where its signature (188 eV) is superimposed to the Si peak (starting at 100 eV), which is the background of the B signal. At any rate, the B seems to be homogenously distributed within the considered grain, at least on the "few nanometer" scale.

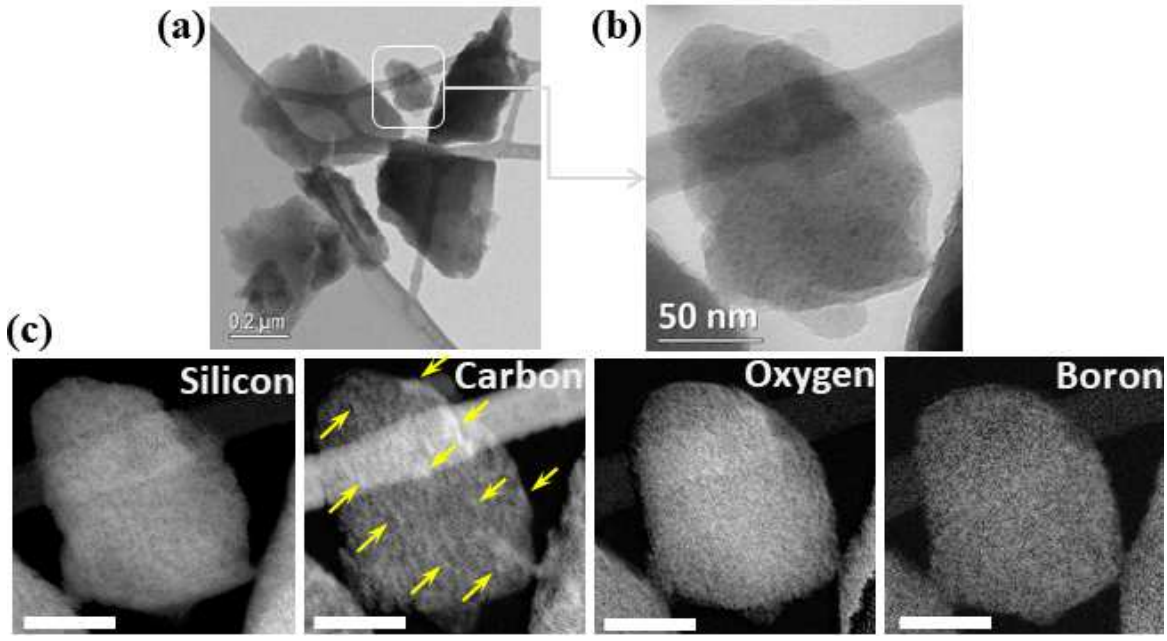


**Figure 4.** (a) General and (b) detailed views of the SiBOC grains prior to the HF treatment. (c) Chemical maps of the elements of interest: Silicon Carbon, Oxygen and Boron, acquired in EFTEM; scalebar: 50 nm.

Since the TEM quotes with the acquisition and exploitation of "projected" micrographs of the objects, the exploration of three-dimensional complex structures and architectures is very difficult by using classical TEM images. In the case of the coexistence of different elements, phases or even nanostructures within the very same volume, the approach commonly adopted is the electron tomography (ET). It allows to probe the inner volumes and/or to assess the distribution of the different phases. In principle, the volume of an area of interest, in this case a grain, is gathered from a series of its projections recorded at different angular orientations with respect to the direction of the electron beam [40, 41]. Afterwards, the electron tomography provides the 3D reconstruction of the area of interest in which the 3D information on the spatial distribution of the compounds in the specimen

is mathematically retrieved by using an adapted reconstruction algorithm. In the case of the SiBOC glasses, three different grains have been analyzed for each specimen, e.g. prior and after the HF treatment, in order to establish a valid statistical pattern.

### 3D internal structure of the SiBOC glass before HF etching

In the first step, 3D TEM analysis has been performed in order to determine the internal microstructure of the as synthetized sample. A careful analysis of the reconstructed volume slice by slice and following different orientations as against the grain orthogonal axes identified the homogenous spatial distribution of denser (SiC) areas inside the aggregate (**Figure 5**). Several slices extracted from the reconstructed volume evidenced the coexistence of regions populated with large size particles located mostly at the grain edges (upper part in Figure 5b) and areas with combined small and large particles, all over the grain section (Figure 5c). In terms of shape, the SiC grains are spherical with small deviations from it, whilst from a statistical point of view, their sizes follows a bimodal distribution with the two maxima at 2.3 ± 0.5 nm and 5 ± 1 nm. It is worth mentioning here that owing to the nature and small size of these nanocrystals, valuable information on their shape and sizes are particularly difficult to achieve by other characterization methodologies. From a quantitative perspective, the number of the SiC crystallites was estimated at about 25 within a volume of $10^4$ $nm^3$, with a ratio of 1:4 between the large to small crystallites. The SiC grain size measured by TEM is in good agreement with the value 2.8 ± 0.2 nm, given by Pena-Alonso et al. [31] as obtained from XRD analysis for a SiBOC glass annealed under the same thermal constraints. Values of SiC size between 2 and 6 nm have also been reported, from XRD studies, for other SiOC and SiBOC glasses pyrolyzed in the temperature range between 1200 and 1500°C [35, 43].

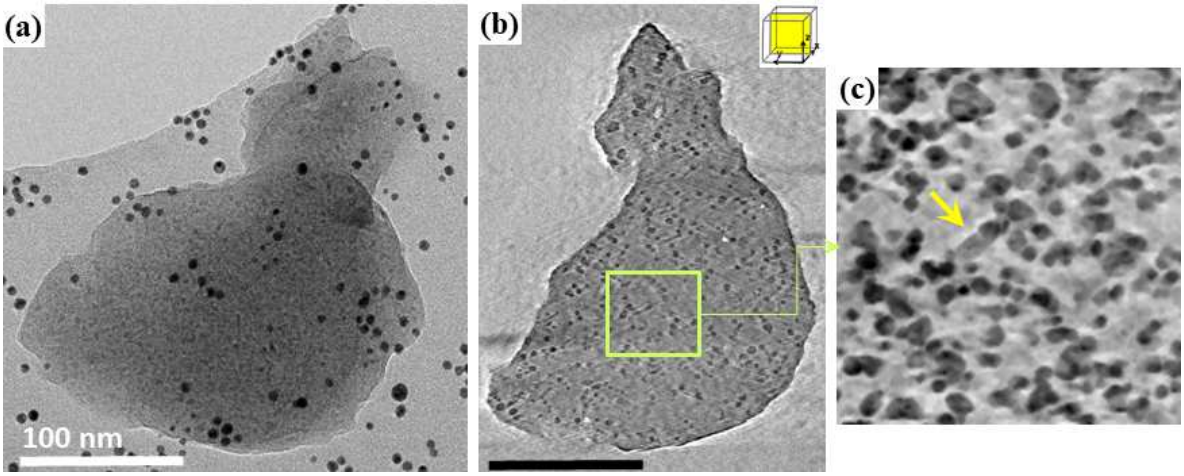


**Figure 5**. Electron tomography of the parent SiBOC sample. (a) As-acquired TEM micrograph extracted from the raw series of images (the dark particles are Au fiducials used for the images fine alignment). (b) General and (c) detailed slices redrawn from the reconstructed volume; the yellow arrow points to a carbon rich area embedded in the SiO2-based matrix (light grey) and SiC NPs (darker particles). Scale bar in (b): 100 nm

The low contrast between the carbon and $SiO_2$-based phases as developed in TEM does not allow to undoubtedly differentiate and further quantify these phases in terms of their relative spatial localization and 3D densities. In this context, the HF etching has been used as methodology to remove the $SiO_2$-rich phase and subsequently provide additional

information, as shown in the second part of the work. However, from the 3D data obtained on the raw specimen, one can unambiguously assign at several locations of the grain the darker platelet-like contrast to the graphitic platelets as identified in both classical 2D TEM micrographs and the slices within the reconstructed volume. The length of such platelets was statistically estimated from the 3D tomograms at about 10 ± 3 nm, whilst their thickness is much smaller and was estimated, by using principally the well visible platelets, at about 2 ± 0.5 nm. This value is in good agreement with the thickness evaluated from the classical TEM images where the platelets-like graphitic structures are constituted of about 7 graphitic planes, as visible at the borders of the considered grains in the Figure 3.

A deeper insight of the internal structure of the grains can be achieved by a more localized observation of several representative slices as represented in **Figure 6**. Here, the SiC crystallites and the C-rich platelets can be unambiguously identified based on their characteristic morphologies.

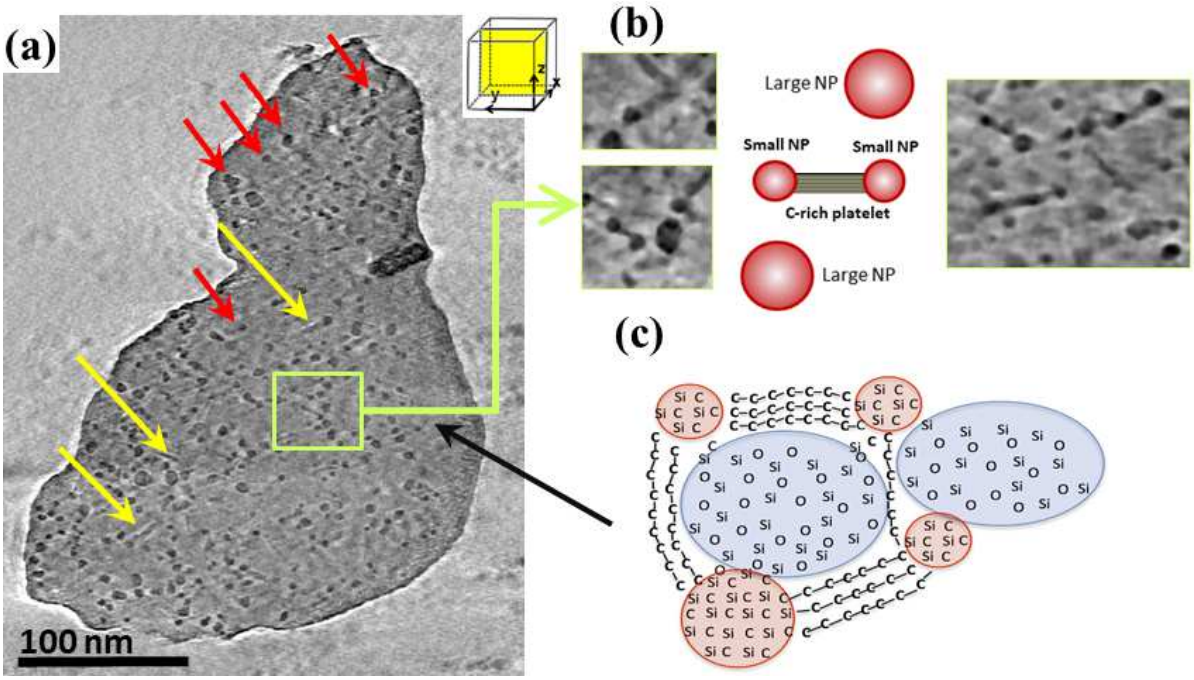


**Figure 6**. (a) Typical slice redrawn from the reconstructed volume; the yellow arrows point to a carbon rich and the red arrows point to SiC NPs areas embedded in $SiO_2$-based glass (light grey). (b) Higher magnification slices of the C-rich platelets bridging the small SiC NPs located in the close vicinity of larger NPs. (c) Schematic representation of the ordering and bonding within the chemically different domains.

Accordingly, the analysis of the tomogram in close vicinity of the well-defined C-rich platelets unraveled a rather striking information: most of the platelet-like structures seem to act as bridges between the small spherical particles previously assigned to the SiC with a mean size of about 2.3 nm (Figure 6). Apart from the creation of bonds between two neighboring particles schematically represented in the central part of Figure 6b, longer bridges can locally form by multi-particles bonding as shown for the case of three particles (right side in Figure 6b). It is important to mention here that this is the first report on the experimental evidence of such bridges connecting the SiC crystallites in the SiBOC grains. As it concerns the clear visualization of the SiC-carbon binding, this finding stand strongly

advocates for the structural model proposed by Gregori et al [14] schematically illustrated in Figure 6c.

As mentioned before, the microstructure of the SiBOC grains was explored by the TEM-based methodology after the HF etching as well. In principle, the HF is prone to preferentially dissolve the $SiO_2$-based phase leading to a sharp change of the contrasts achieved under the impact of the electron beam from the TEM. The contrasts within the TEM-based micrographs are expectedly more pronounced and therefore the analysis of the material structural characteristics in terms of the spatial distribution of the SiC and C graphitic platelets becomes straightforward both under 2D and 3D.

**2D microstructure of the SiBOC glass after the HF etching**

The first information earned by the classical TEM analysis is the grains porosity and subsequent loss of the structure density as compared to the starting SiBOC grains, attributed to the etching of the $SiO_2$-based nano-phase. A more detailed analysis by high resolution HAADF-STEM identifies the occurrence of the SiC crystallites as well as of the carbon graphitic platelets (**Figure 7**). The latter appear to generally connect two neighboring SiC particles. From a qualitative point of view, a careful evaluation of the images points to a larger thickness of the platelets than for the case of the non-etched specimen.

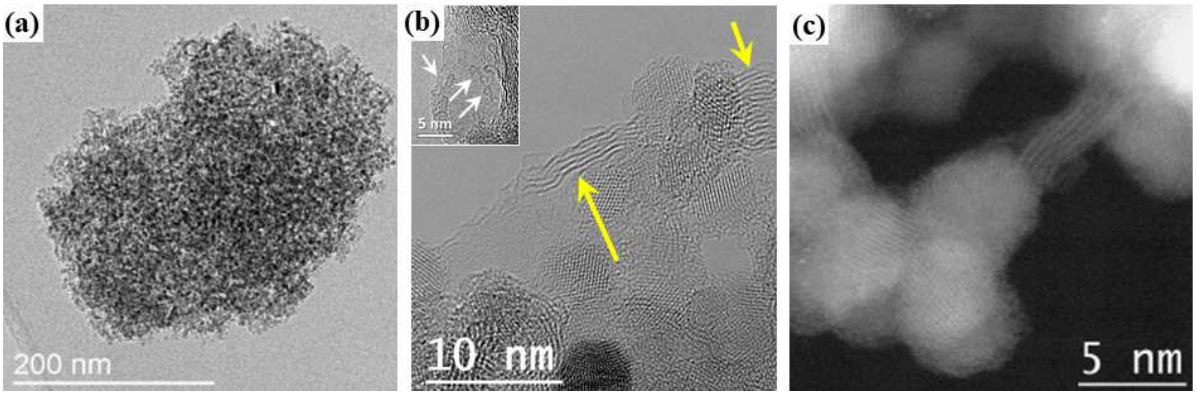


**Figure 7**. TEM micrographs of the SiBOC glasses after HF etching treatment. (a) General aspect of one agglomerate constituted by (b) SiC nanograins with sizes smaller than 10 nm and graphitic structures indicated by the yellow arrows. The white arrows in the HR image from the inset points to surface defects commonly identified on the surface of graphene sheets (c) HR STEM HAADF image of nanoparticles connected by graphitic structures.

The analysis of the high resolution images shown a lower density of the crystallographic defects than in the parent sample, e.g. before the HF treatment, which can be seen as an increase of the graphitization degree. This is confirmed in the first place by the measured distance between the graphitic planes, 0.34 nm, which is very close to the corresponding distance in graphite structures. Secondly, the exploration of the fine structure of the C-edge as acquired by Electrons Energy Loss Spectroscopy (EELS) in TEM allowed one to identify the spectral imprint of the C sp2 within the platelets, as shown in **Figure 8**. The high spatial resolution is achieved by STEM and it allows to gather a complete image on the distribution of the two principal residual components, the graphitic carbon and the SiC, along a well-defined “line profile”. Indeed, the Si and C content vary along the scanning direction indicated by the arrows in Figure 8. Such, at the edge of the investigated area, the Si content is high suggesting the presence of a SiC nanoparticle with a 6 nm diameter,

which can be identified on both the image in Figure 8a and the elements concentration profile in Figure 8b. As expected, the C K-edge evolves along the scanning line as the spectra from the SiC area marked by two equally height smooth peaks is replaced by a two-peak spectra (shown in the inset). The specific allure of a $sp^2$ carbon graphitic system exhibit a pre-peak located at 284eV and a smoother peak situated at about 290eV with an intense inner peak at low energy [39].

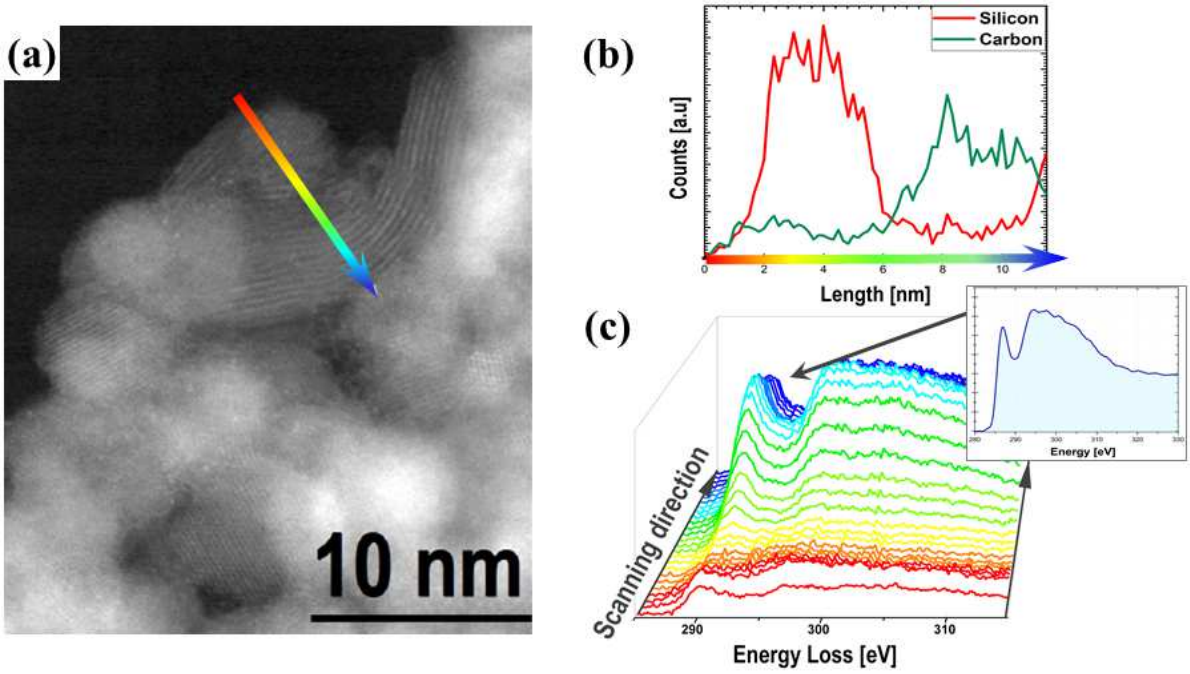


**Figure 8**. Spectrum imaging analysis (STEM-EELS) of the SiBOC glass after HF treatment. (a) STEM-HAADF micrograph of the region chosen for the line scan along the direction indicated. (b) The variation of the C and Si content and (c) the Carbon (K edge) fine structure evolution along the scanning direction. Note: the colors in the graphical representation above were randomly chosen.

A complementary analysis by EFTEM at the Si-K and C-K edges confirms the heterogeneous distribution of the C-rich and Si-rich area within the HF treated specimen at larger extent, as displayed in Figure 9 (a and b). In the case of the boron distribution within the HF etched SiBOC glass, the model retrieved mostly in the literature [31, 37] stipulates that the B atoms which are not etched out with the $SiO_2$ are retained principally by the C $sp^2$ rich areas forming $BC_3$ units. However, given the small amount of residual B in the treated specimen (ca 0.9 wt%), a complete analysis of the B elemental map in relation with the C and Si maps by EFTEM is not conclusive. Therefore, cumulative spectra were acquired in two different areas of the grains: a SiC-rich and a C-graphitic predominant regions. Although small amounts of B were detected in both types of locations, no significant difference was identified.

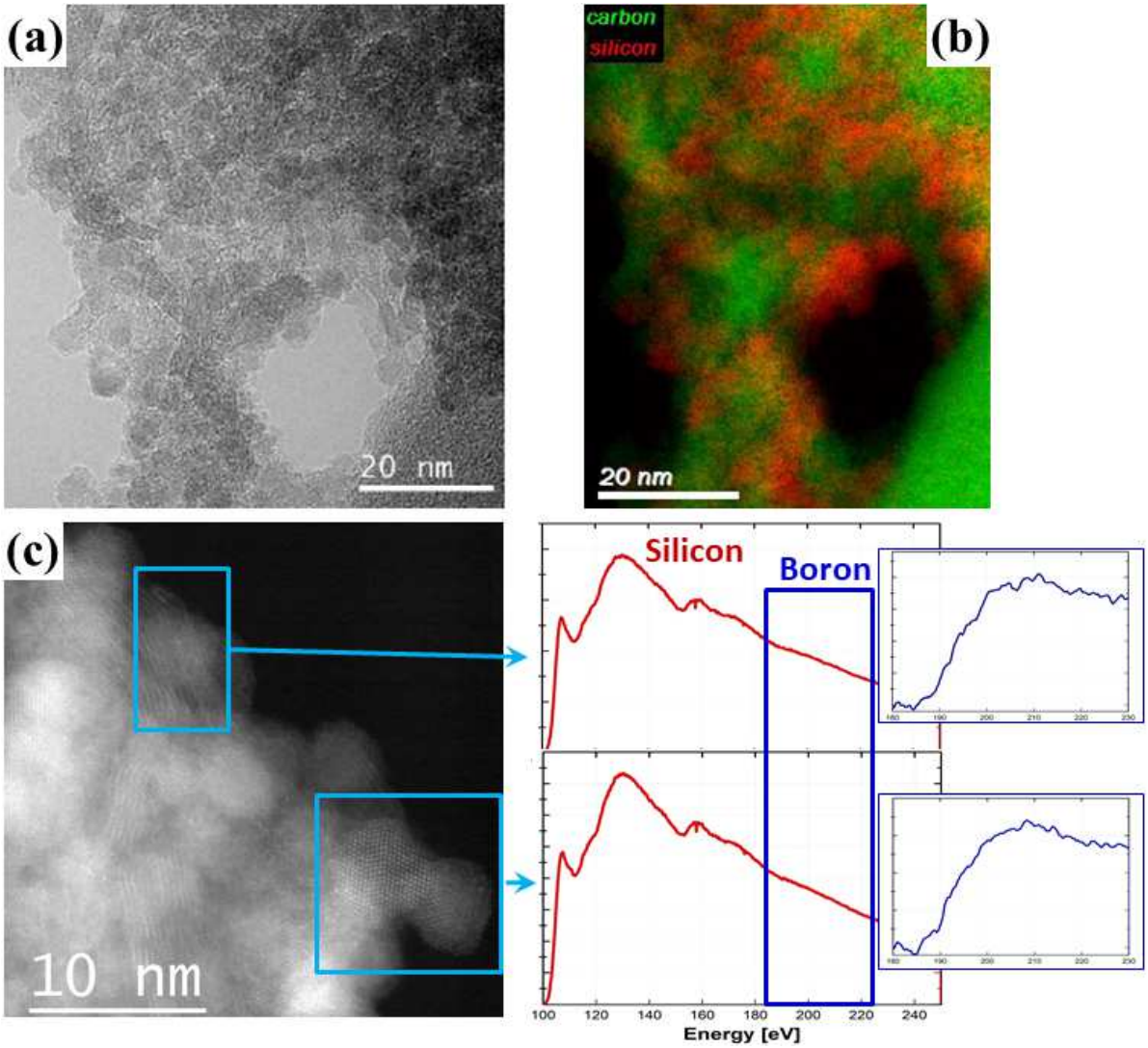


**Figure 9.** (a) Typical zero loss energy filtered TEM (elastically scattered electrons) micrograph and (b) superposition of the C and Si maps of a representative area within the HF treated SiBOC glass. (c) STEM-HAADF image and the selection of the regions chosen for the acquisition of cumulative energy loss spectra displayed on the right side; the insets represent the B spectra (rectangle in the Si signal) after background removal.

### 3D structure of the Si(B)OC glass after the HF etching

Similar with the case of the parent specimen, the 3D TEM analysis by ET provides unprecedented information on the internal structure of the SiBOC glass particularly after the HF etching as the $SiO_2$-based phase was dissolved. Therefore we take advantage of the augmented contrasts and signal to noise ratio in the reconstructed volume. The analysis of the reconstructed volume slice by slice reveals the coexistence of spherical grains, platelets and voids (**Figure 10**). Based on the previous 2D TEM analyses, we can assign the granular morphology to the SiC nanocrystals which appear as spherical particles, locally faceted. The C-rich nanophase exhibit a platelets-like morphology as discussed previously, whereas the voids can be associated to the initial localization of the silica-based phase. The general view identifies a rather continuous network of SiC and C-free after etching, as predicted by the models advanced in the literature [12, 14, 15]. The two types of grains, e.g. SiC and elongated C platelets are locally but randomly connected. The direct visualization of the morphology of the various platelets from the volume allowed one to statistically estimate

their sizes after the HF etching as about 2.8 ± 0.7 nm, which is larger than the corresponding value before the HF attack (2 ± 0.5 nm).

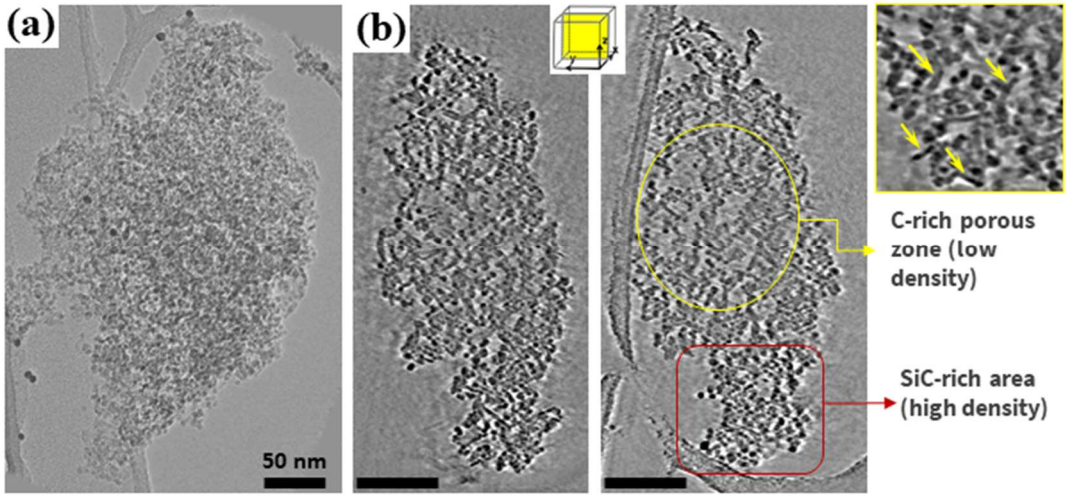


**Figure 10.** Electron tomography of the HF-etched SiBOC sample. (a) TEM micrograph acquired during the series acquisition. (b) General and detailed slices redrawn from the reconstructed volume identifying the high porosity of the C-rich areas and the 3D agglomeration of the SiC nanoparticles.

Apart from the network created by the SiC grains and the graphitic platelets, the microstructure of this specimen is marked by a bimodal distribution of the porosity. This can be correlated with the presence of regions with different densities. Such, one observes regions of high concentrations of spherical SiC particles (delimited by the red rectangle) and areas rich in graphitic platelets (encircled by the yellow mark). The densities of these regions are different as the stacking of the constituents is mostly dictated by the geometry of the constituents, such that the porosity is “higher” in the areas characterized by a higher concentration of graphitic platelets. A rough estimation of the mean pore diameters in the two areas reveals 5 nm for the SiC-area and 10 nm for the platelets-area, values which are close to the results obtained by the $N_2$ physisorption analysis.

## 4. Discussion

By comparing the specimens prior and after the HF etching treatment, we conclude that, in addition to the silica dissolution, a restructuration of the initial roughly graphitic layers occurs during the process via a sharp reorganization of the $sp^2$ C planes and most probably due to the local diffusion and reorientation of the individual graphitized C lamellar structures. The ordering process of the free carbon phase during HF etching was already proposed in the literature based on Raman data [25] and from in-situ X-ray diffraction studies [43]. In this last paper [43], it was shown that the ordering process leads to a decrease of the $sp^2$ basal spacing of the free carbon phase toward the typical value of graphite in good agreement with the present results. This restructuration of the $sp^2$ C layers reported herein and induced by the HF attack suggests that the graphene layers within the SiOC nanostructure possess certain degree of mobility. Accordingly, from the two possible nanostructure models, the one which should provide the higher mobility/flexibility to the graphene layers is that in which the layers are bonded to the matrix via Si-C bonds only at the edges of the layers rather than having covalent C-Si bonds in the C-planes oriented in orthogonal direction, as proposed by the other model. The

model of the $sp^2$-C planes bonded through their edges is supported by the experimental evidence obtained for the first time in this work showing the graphitic platelets bridging two and/or more neighboring SiC nanograins (**Figures 6 and 8**) and forming a continuous C-rich domain, interpenetrating the silica-rich domain. The SiC nanocrystals bonded to the $sp^2$ layers are smaller (2.3 nm) that the SiC nanocrystals which are not bonded to the graphitic platelets (5.0 nm). Silicon carbide crystals which are involved in a chemical bond with the graphene layers could be less mobile and therefore less prone to crystal growth as compared to the SiC crystals not bonded to the graphitic platelets. Finally, we observed that the volumes of the particles with the higher density of graphitic platelets (and lower density of SiC crystals) are more porous and the pores close to the C phase seem larger compared to the other zones of the sample. This observation could be rationalized by assuming that the $SiO_2$-based network is not bonded with the carbon $sp^2$ basal planes and, accordingly, is free to reorganize and grow into larger amorphous clusters which are subsequently removed by HF and form the observed porosity. Conversely, the silica glass which is in close proximity with the SiC nanocrystals must be chemically bonded to the SiC phase via Si-C bonds and therefore its rearrangement to give large $SiO_2$-based clusters must be hindered.

## 5. Conclusions

The nanostructure of SiBOC glasses pyrolyzed at 1400°C was deeply investigated, before and after HF etching, with a combination of TEM-based techniques, including high resolution, EELS spectroscopy and electron tomography. Accordingly, for the first time, the 3D internal nanostructure of the silicon-boron-oxycarbide glasses was unveiled. The main results are as follows: *i)* the SiBOC glass contains an amorphous silica-based phase, SiC nanocrystals, which have a bimodal size distribution (2.3 ± 0.5 and 5 ± 1 nm, with a 4:1 ratio between them), and graphitic nanoplatelets with a lateral size of 10 ± 3 nm and thickness of 2 ± 0.5 nm; these components are assembled into two interpenetrating nano-sized networks, one silica-rich and the other one C-rich; *ii)* most of the graphitic platelets connect two silicon carbide nanocrystals (mainly the smaller SiC nanocrystals) via chemical bonds at the edge of the $sp^2$ planes; *iii)* HF etching leads to the formation of a porous network in which the pores in close proximity to the graphitic platelets are larger compared to the pores formed in regions with higher density of SiC nanocrystals; this observation may be rationalized by assuming that no Si-C bonds exist between the $SiO_2$-based glass and the $sp^2$ basal planes of the graphitic platelets; conversely, the pores in close proximity of the SiC nanocrystals are smaller since the Si-C bonds present at the interface hinder the reorganization of the glass into larger amorphous clusters.

## 6. Acknowledgments

GENESIS is supported by the Région Haute-Normandie, the Métropole Rouen Normandie, the CNRS via LABEX EMC and the French National Research Agency as a part of the program “Investissements d’avenir” with the reference ANR-11-EQPX-0020.

## References


[1] C. G. Pantano, A. K. Singh, H. Zhang, "Silicon Oxycarbide Glasses", *J. Sol-Gel Sci. Technol.,* **14** (1999), 7-25.

[2] C. Stabler, E. Ionescu, M. Graczyk-Zajac, I. Gonzalo-Juan, R. Riedel, "Silicon oxycarbide glasses and glass-ceramics: "All-Rounder" materials for advanced structural and functional applications", *J Am Ceram Soc.* **101** (2018), 4817-4856.

[3] G. M. Renlund, S. Prochazka and R. H. Doremus, "Silicon oxycarbide glasses: Part II. Structure and properties", *J. Mater. Res.* **6** (1991), 2723-2734.

[4] T. Rouxel, G. Massouras and G. D. Sorarù, "High Temperature Behavior of an SiOC Oxycarbide Glass: Elasticity and Viscosity", *J. Sol-Gel Sci. Technol.* **14** (1999), 83-94.

[5] H. Bréquel, J. Parmentier, S. Walter, R. Badheka, G. Trimmel, S. Masse, J. Latournerie, P. Dempsey, C. Turquat, A. Desmartin-Chomel, L. Le Neindre-Prum, U.A. Jayasooriya, D. Hourlier, H.-J. Kleebe, G. D. Sorarù, S. Enzo, F. Babonneau, "Systematic structural characterisation of the high temperature behaviour of nearly-stoichiometric silicon oxycarbide glasses", *Chem. Mater.* **16** (2004), 2585-2598.

[6] R. J. E Corriu, D. Leclercq, P.H. Mutin, A. Vioux, "Preparation and Structure of Silicon Oxycarbide Glasses Derived from Polysiloxane Precursors", *J. Sol-Gel Sci. Technol.* **8** (1997), 327-330.

[7] G. T. Burns, R. B. Taylor, Y. Xu, A. Zangvil, G. A. Zank, "High-Temperature chemistry of the conversion of Siloxanes to Silicon Carbide", *Chem. Mater.* **4** (1992) 1313-1323.

[8] G. D. Sorarù, G. D'Andrea, R. Campostrini, F. Babonneau, G. Mariotto, "Structural Characterization and High Temperature Behaviour of Silicon Oxycarbide Glasses Prepared from Sol-Gel Precursors Containing Si-H Bonds", *J. Am. Ceram. Soc.* **78** (1995), 379-387.

[9] F. Roth, P. Waleska, C. Hess, E. Ionescu, N. Nicoloso, "UV Raman spectroscopy of segregated carbon in silicon oxycarbides", *J. Ceram. Soc. Japan* **124** (2016), 1042-1045.

[10] L. Bois, J. Maquet, F. Babonneau, H. Mutin, D. Bahloul, "Structural Characterization of Sol-Gel Derived Oxycarbide Glasses. 1. Study of the Pyrolysis Process", *Chem. Mater.* **6** (1994), 796-802.

[11] S. Dirè. E. Borovin, M. Narisawa, G. D. Sorarù, "Synthesis and Characterization of the First Transparent Silicon Oxycarbide Aerogel Obtained Through $H_2$ Decarbonization", *J Mater. Chem. A* **3** (2015), 24405-24413.

[12] A. Saha, R. Raj, D. L. Williamson and H.-J. Kleebe, "Characterization of Nanodomains in Polymer-Derived SiCN Ceramics Employing Multiple Techniques", *J. Am. Ceram. Soc.* **88** (2005), 232-234.

[13] L. Yu, R. Raj, "On the thermodynamically stable amorphous phase of polymerderived silicon oxycarbide", *Scientific Reports,* DOI: 10.1038/srep14550.

[14] G. Gregori, H.-J. Kleebe, Y. D. Blum and F. Babonneau, "Evolution of C-rich SiCO ceramics. Part II. Characterization by high lateral resolution techniques electron energy-loss spectroscopy, high-resolution TEM and energy-filtered TEM", *Int. J. Mater. Res.* **97** (2006) 710-720.

[15] S. J. Widgeon, S. Sen, G. Mera, E. Ionescu, R. Riedel, A. Navrotsky, "$^{29}$Si and $^{13}$C Solid-State NMR Spectroscopic Study of Nanometer-Scale Structure and Mass Fractal Characteristics of Amorphous Polymer Derived Silicon Oxycarbide Ceramics", *Chem. Mater.* **22** (2010), 6221–6228.

[16] P. Kroll, "Modeling the "free carbon" phase in amorphous silicon oxycarbide", *J. Non-Cryst. Solids* **351** (2005), 1121–1126.

[17] P. Kroll, "Searching insight into the atomistic structure of SiCO ceramics", *J. Mater. Chem.,* **20** (2010) 10528-10534.

[18] T. Varga, A. Navrotsky, J.L. Moats, R.M. Morcos, F. Poli, K. Muller, A. Sahay, and R. Raj, "Thermodynamically stable SixOyCz polymer-like amorphous ceramics", *J. Am. Ceram. Soc*. **90** (2007), 3213-3219.

[19] A. H. Tavakoli, M. M. Armentrout, S. Sen, A. Navrotsky, "Hydrogenated Si–O–C nanoparticles: Synthesis, structure, and thermodynamic stability", *J. Mater. Res.* **30** (2015), 297-303.

[20] H. Fukui, Y. Harimoto, M. Akasaka, K. Eguchi, "Lithium species in electrochemically lithiated and delithiated silicon oxycarbides", *ACS Appl. Mater. Interfaces* **6** (2014), 12827–12836.

[21] R. Riedel, L. Toma, E. Janssen, J. Nuffer, T. Melz, H. Hanselka, "Piezoresistive Effect in SiOC Ceramics for Integrated Pressure Sensors", *J. Am. Ceram. Soc.* **93** (2010), 920-924.

[22] M. Graczyk-Zajac, D. Vrankovic, P. Waleska, C. Hess, P. Vallachira Sasikumar, S. Lauterbach, H.-J. Kleebe, G. D. Sorarù, "The Li-storage Capacity of SiOC Glasses with and without Mixed Silicon Oxycarbide Bonds", *J. Mater. Chem. A* **6** (2018), 93-103.

[23] C. Stabler, D. Schliephake, M. Heilmaier, T. Rouxel, H.-J. Kleebe, M. Narisawa, R. Riedel, E. Ionescu, "Influence of SiC/Silica and Carbon/Silica Interfaces on the High-Temperature Creep of Silicon Oxycarbide-Based Glass Ceramics: A Case Study", *Adv. Eng. Mater.* (2018), 1800596.

[24] A. M. Wilson, G. Zank, K. Eguchi, W. Xing, B. Yates and J. R. Dahn, "Pore Creation in Silicon Oxycarbides by Rinsing in Dilute Hydrofluoric Acid", *Chem. Mater*. **9** (1997)**,** 2139-2144.

[25] R. Peña-Alonso, G. D. Sorarù and R. Raj, "Preparation of Ultrathin-Walled Carbon-Based Nanoporous Structures by Etching Pseudo-Amorphous Silicon Oxycarbide Ceramics", *J. Am. Ceram. Soc.* **89** (2006), 2473–2480.

[26] H.-Y. Kleebe, Y. D. Blum, "SiOC ceramic with high excess free carbon", *J. Europ. Ceram. Soc.,* **28** (2008), 1037–1042.

[27] L. Biasetto, R. Pena-Alonso, G. D. Soraru, P. Colombo,"Etching of SiOC ceramic foams", *Advan. Appl. Ceramics* **107** (2008), 106-110.

[28] J. Li, K. Lu, T. Lin, F. Shen, "Preparation of Micro-/Mesoporous SiOC Bulk Ceramics", *J. Am. Ceram. Soc.* **98** (2015), 1753–1761.

[29] C. Vakifahmetoglu, M. Buldu, A. Karakuscu, A. Ponzoni, D. Assefa, G. D. Soraru, "High surface area carbonous components from emulsion derived SiOC and their gas sensing behavior", *J. Europ. Ceram. Soc.* **35** (2015), 4447-4452.

[30] M. Ma, H. Wang, M. Niu, L. Su, X. Fan, J. Deng, Y. Zhang, X. Du, "High rate capabilities of HF-etched SiOC anode materials derived from polymer for lithium-ion batteries", *RSC Adv.* **6** (2016), 43316-43321.

[31] R. Pena-Alonso, G. Mariotto, C. Gervais, F. Babonneau, G. D. Soraru, "New Insights on the high temperature nanostructure evolution of SiOC and B-doped SiBOC Polymer-derived Glasses", *Chem. Mater.* **19** (2007), 5694-5702.

[32] G. D. Soraru, R. Pena-Alonso, H.-J. Kleebe, "The effect of annealing at 1400°C on the structural evolution of porous C-rich silicon (boron)oxycarbide glass", *J. Europ. Ceram. Soc.* **32** (2012), 1751-1757.

[33] H. Wu, J. Yang, H. Chen, F. Pan, "Revealing the nanodomain structure of silicon oxycarbide via preferential etching and pore analysis", *Funct. Mater. Lett.* **9** (2016), 1650043.

[34] C. Gervais, F. Babonneau, N. Dallabona and G.D. Soraru, "Sol-Gel-derived Silicon-Boron Oxycarbide Glasses Containing Mixed Silicon Oxycarbide ($SiC_xO_{4-x}$) and Boron Oxycarbide ($BC_yO_{3-y}$) Units", *J. Am Ceram. Soc.,* **84** (2001) 2160-2164.

[35] M.A. Schiavon, C. Gervais, F. Babonneau, G.D. Soraru, "Crystallization Behaviour of Novel Silicon-Boron-Oxycarbide Glasses", *J Am Ceram Soc.* **87** (2004), 203-208.

[36] A. H. Tavakoli, R. Campostrini, C. Gervais, F. Babonneau, J. Bill, G. D. Sorarù, A. Navrotsky, "Energetics and Structure of Polymer Derived Si-(B-)O-C Glasses: Effect of the Boron Content and Pyrolysis Temperature", *J. Am. Ceram. Soc.* **97** (2014), 303-309.

[37] G. D. Sorarù, G. Kacha, R. Campostrini, A. Ponzoni, M. Donarelli, A. Kumar, G. Mariotto, "The effect of B-doping on the electrical conductivity of polymer-derived Si(B)OC ceramics", *J. Am. Ceram. Soc.* **100** (2017), 4611-21.

[38] C. Pilger, E Leis, P. Tschopel, J. A. C. Broekaert, G. Tolg, "Analysis of silicon carbide powders with ICP-MS subsequent to sample dissolution without and with matrix removal", *Fresenius J. Anal. Chem.,* **351** (1995) 110-116.

[39] G. D. Soraru, R. Campostrini, A.A. Ejigu, E. Zera and P. Jana, "Processing and characterization of polymer derived SiOC foam with hierarchical porosity by HF etching", *J. Ceram. Soc. Jap.* **124** (2016), 1023-1029.

[40] O. Ersen, I. Florea, C. Hirlimann, C. Pham-Huu, "Exploring nanomaterials with 3D electron microscopy", *Materials Today* **18** (2015), 395.

[41] I. Florea, L. Roiban, C. Hirlimann, F. Tihay, C. Pham-Huu, J. Werckmann, C. Pham, P. Nguyen, M. Drillon, O. Ersen, "3D-TEM Characterization of the Porosity in nanoscaled materials: application to catalysis", *Advanced Engineering Materials* **13** (2011), 122.

[42] A. C. Y. Liu, R. Arenal, D. J. Miller, X. Chen, J. A. Johnson, O. L. Eryilmaz, A. Erdemir, J. B. Woodford, "Structural order in near-frictionless hydrogenated diamondlike carbon films probed at three length scales via transmission electron microscopy", *Physical Review B* **75** (2007), 205402.

[43] G. D. Soraru, R. Pena-Alonso, M. Leoni, "C-rich micro/mesoporous Si(B)OC: in situ diffraction analysis of the HF etching process", *Microp. Mesop. Mater.* **172** (2013), 125-130.